

## 1. 2016 Research Program

In 2016, the Laboratory continued the realization of Theme 04-9-1077-2009/2017 "Research on the Biological Effect of Heavy Charged Particles with Different Energies" in the following fields: fundamental radiobiological and radiation genetics research with heavy charged particles; research on the action of accelerated charged particles on the central nervous system and eye structures; mathematical modeling of radiation-induced effects; and radiation research at JINR's basic facilities and in the environment. Work was continued on Theme 04-9-1112-2013/2016 "Research on Cosmic Matter on the Earth and in Nearby Space; Research on the Biological and Geochemical Specifics of the Early Earth."

## 2. 2016 Research Results

### 2.1. *Radiation Genetics and Radiobiology*

Research was continued on the regularities of the induction and repair of DNA double-strand breaks (DSBs) in normal human fibroblast cells after exposure to ionizing radiations with different physical characteristics [1-4]. Experiments were repeated on cell irradiation with  $^{60}\text{Co}$   $\gamma$ -rays to refine the dose dependences of DNA DSB induction and to analyze the complexity of clustered  $\gamma\text{H2AX}/53\text{BP1}$  foci and kinetics of their morphology change. At the U400M accelerator (the Laboratory of Nuclear Reactions, JINR), normal human fibroblasts were irradiated with  $^{11}\text{B}$  ions with energies of 32.3 and 13.5 MeV/nucleon and the respective linear energy transfer (LET) values of 44.6 and 91.5 keV/ $\mu\text{m}$  and  $^{20}\text{Ne}$  ions with an energy of 46.6 MeV/nucleon and LET of 132.1 keV/ $\mu\text{m}$ . Cells were irradiated in two geometries: normally to the beam to study the dose dependence and kinetics of DNA DSB repair, and tangentially (at an angle of 10 degrees) to study the tracks formed by  $\gamma\text{H2AX}/53\text{BP1}$  foci in cell nuclei, their clustering degree, and their morphology change. The irradiated cells were fixed at different times after exposure and immunofluorescent staining was performed to detect the  $\gamma\text{H2AX}$  and 53BP1 proteins — DNA DSB repair markers. A comparative analysis was performed between the obtained data and the results of earlier experiments on the irradiation of fibroblasts with  $^{11}\text{B}$  ions with an energy of 8.1 MeV/nucleon and LET of 138.1 keV/ $\mu\text{m}$ . It was shown that the kinetics of the formation and elimination of  $\gamma\text{H2AX}/53\text{BP1}$  foci is different and depends on the physical characteristics of a specific ionizing radiation.

A dose dependence was obtained of  $\gamma\text{H2AX}/53\text{BP1}$  foci induction in human fibroblasts 1 h after irradiation with  $^{60}\text{Co}$   $\gamma$ -rays and accelerated  $^{11}\text{B}$  and  $^{20}\text{Ne}$  ions. For all types of radiation used in the study, a linear dependence is observed at low doses, which is characteristic of the dose

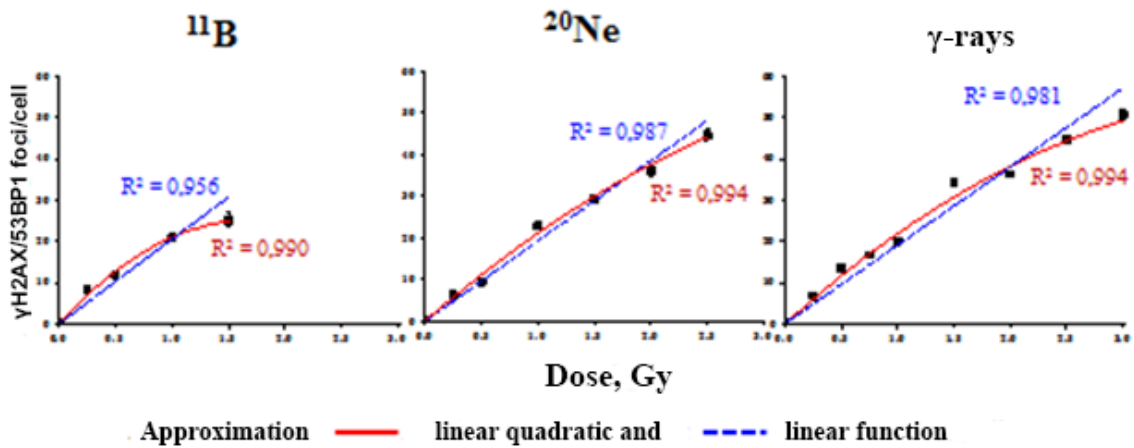


**Fig. 1.** Dose dependences of  $\gamma$ H2AX/53BP1 foci induction in human fibroblast nuclei 1 h after irradiation with accelerated  $^{11}\text{B}$  and  $^{20}\text{Ne}$  ions and  $^{60}\text{Co}$   $\gamma$ -rays in the normal geometry.

dependence of DNA DSB formation. However, with increasing the dose, a deviation from linearity takes place, which can be accounted for by the experimental techniques (Fig. 1).

For both types of accelerated heavy ions, a delay of the kinetics of  $\gamma$ H2AX/53BP1 foci elimination — i.e., DNA DSB repair — was observed compared with  $\gamma$ -rays. It was shown that 4 h after heavy ion irradiation, 85% of the maximal  $\gamma$ H2AX/53BP1 foci level remains in cells, while for  $\gamma$ -irradiation, 41%. It was also found that in the case of  $^{20}\text{Ne}$  ion exposure,  $\gamma$ H2AX/53BP1 foci elimination proceeds much slower than for  $^{11}\text{B}$  ions, which is probably connected with a higher complexity of the foci and, therefore, with more difficult repair of DNA DSBs induced by neon ions. 24 hours after  $\gamma$ -exposure, radiation-induced foci yield decreases to a minimum of 6%; for boron ion exposure, to 26%; while for neon ion irradiation, 45% of the  $\gamma$ H2AX/53BP1 foci remains (Fig. 2). These conclusions agree with the results obtained on the cells irradiated tangentially at an angle of 10 degrees. It was established that the size (area) and complexity (the shape and number of the individual foci in a cluster) of the  $\gamma$ H2AX/53BP1 foci are much greater for neon ion exposure (Fig. 3).

A study was started of the regularities in the formation and repair of DNA DSBs in rat brain neurons after exposure to ionizing radiations of different quality. An immunohistochemical analysis-based technique was developed and refined of detecting  $\gamma$ H2AX/53BP1 foci in paraffin sections of rat brain tissues prepared with the help of an electronic rotary microtome (HM 340E, Thermo Fisher Scientific). To study the dose dependence and kinetics of the induction and elimination of  $\gamma$ H2AX/53BP1 foci after exposure to  $^{60}\text{Co}$   $\gamma$ -rays, female Sprague — Dawley rats (11 weeks old, weighing 220 g) were cranially irradiated at doses of 1, 3, and 5 Gy; 1, 4, and 24 h afterwards, they were decapitated and subsequent analysis was performed.

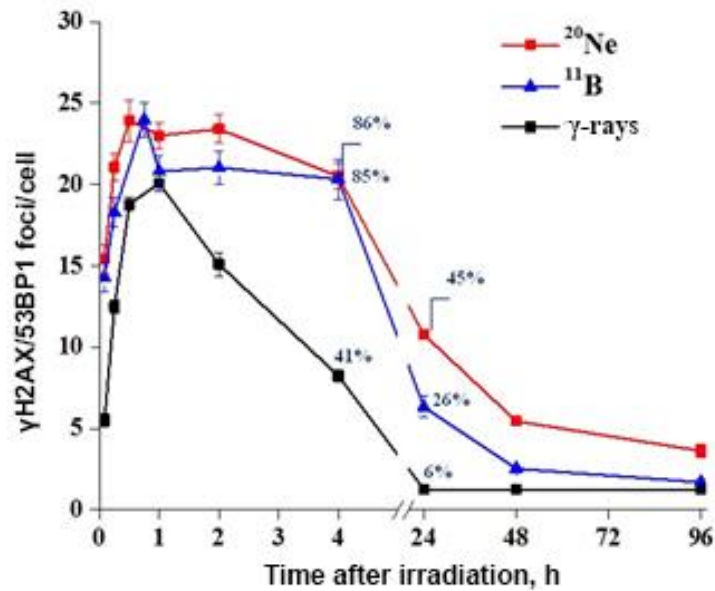


**Fig. 2.** Kinetics of the formation and elimination of  $\gamma\text{H2AX}/53\text{BP1}$  foci in human fibroblast nuclei after irradiation with accelerated  $^{11}\text{B}$  and  $^{20}\text{Ne}$  ions and  $^{60}\text{Co}$   $\gamma$ -rays.

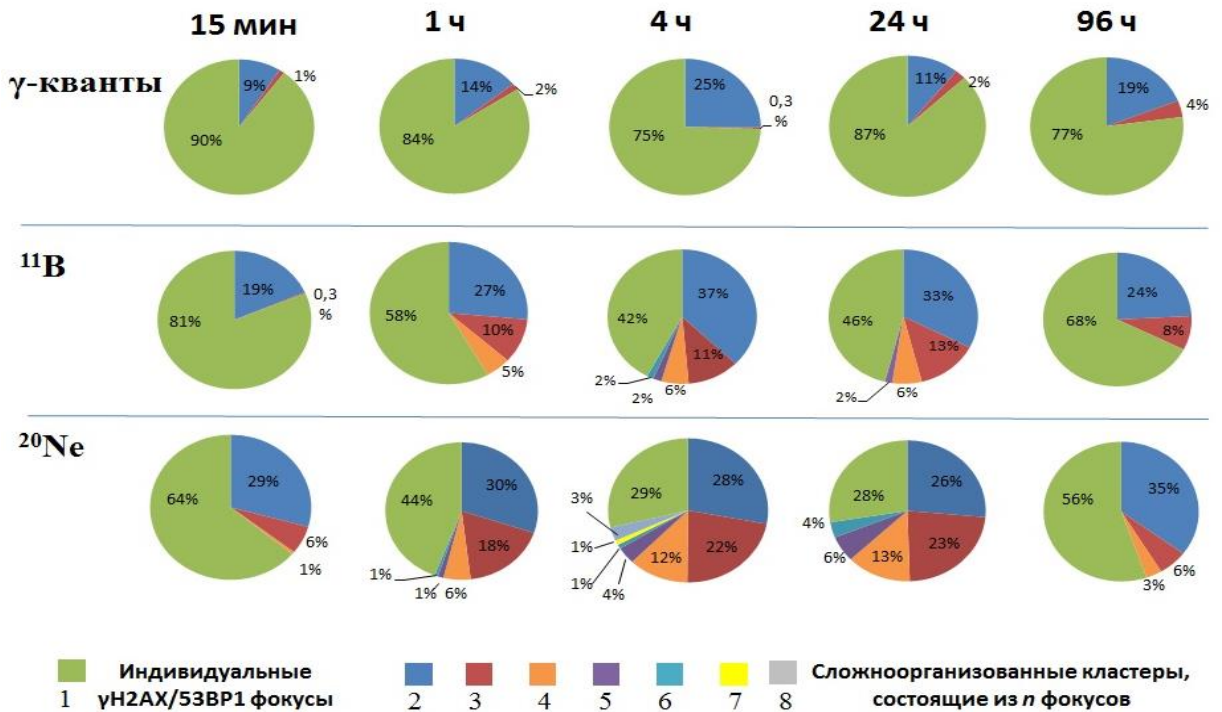


**Fig. 3.** Histograms of the kinetics of complex clustered  $\gamma\text{H2AX}/53\text{BP1}$  foci structure change for irradiation with accelerated  $^{11}\text{B}$  and  $^{20}\text{Ne}$  ions and  $^{60}\text{Co}$   $\gamma$ -rays.

Research was continued on the regularities in the formation and repair of DNA DSBs of different genesis — direct and enzymatic — after exposure to ionizing radiations with different LET in the presence of repair inhibitors cytosine arabinoside (AraC) and hydroxyurea (HU) in human peripheral blood lymphocytes. Dose dependences were obtained for DSB induction by  $^{60}\text{Co}$   $\gamma$ -rays and accelerated  $^{11}\text{B}$  ions with LET of 44, 89, and 127 keV/ $\mu\text{m}$ ; they have a linear character both in normal conditions and in the presence of DNA repair inhibitors (Fig. 4).

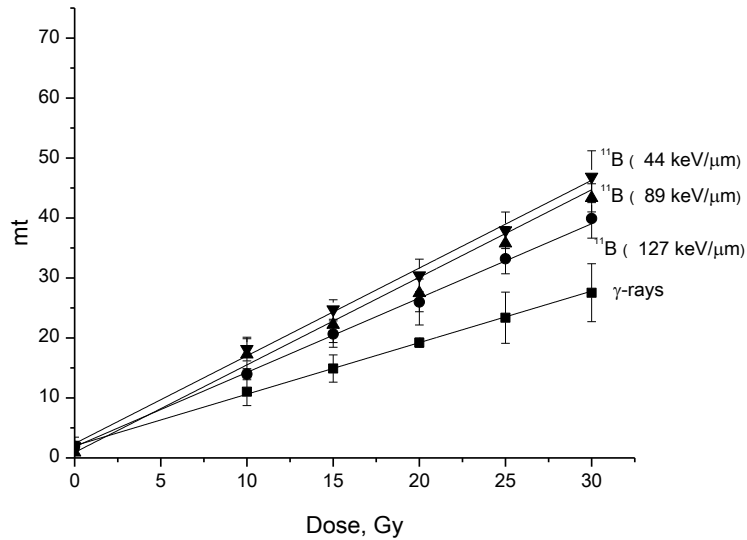


**Fig. 4.** Dose dependences of DNA DSB induction by accelerated  $^{11}\text{B}$  ions with LET of 44, 89, and 127 keV/ $\mu\text{m}$  and  $^{60}\text{Co}$   $\gamma$ -rays.

It was shown that for both  $\gamma$  and accelerated  $^{11}\text{B}$  ion exposure, DNA DSB yield decreases exponentially in the course of repair and practically ends after 6 h of post-irradiation incubation.

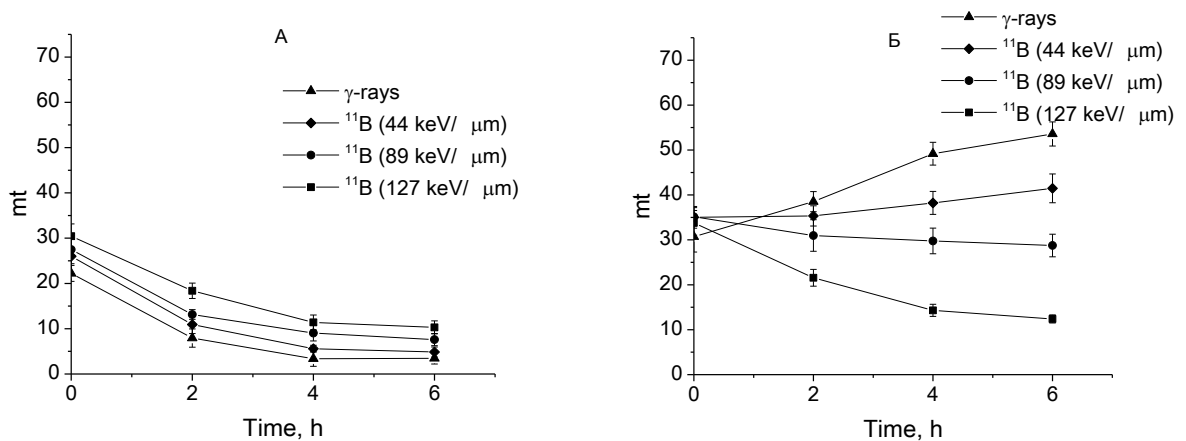


**Fig. 5.** Kinetics of DNA DSB repair after exposure to  $\gamma$ -rays and  $^{11}\text{B}$  ions with different LET at a dose of 20 Gy in normal conditions (A) and in the presence of AraC+HU (B).

In the presence of inhibitors, an increase in DNA DSB yield is observed for exposure to  $\gamma$ -rays and  $^{11}\text{B}$  ions with LET of 44 keV/ $\mu\text{m}$ ; and a slight decrease in DNA DSB yield is observed for irradiation with ions with LET of 89 keV/ $\mu\text{m}$ . With increasing LET to 127 keV/ $\mu\text{m}$ , a decrease in DNA DSB yield with exponential kinetics is observed — like in the absence of repair inhibitors (Fig. 5).

With the use of the fluorescent immunocytochemical staining method, specifics were studied of the formation of direct and enzymatic DNA DSBs in human fibroblasts exposed to  $^{60}\text{Co}$   $\gamma$ -rays at a dose of 1 Gy — in normal conditions and in the presence of the repair inhibitors AraC and HU. It was shown that in the normal conditions, the maximal yield of radiation-induced  $\gamma\text{H2AX}/53\text{BP1}$  foci takes place 1 h after exposure; 4 h afterwards, most of the foci — about 80% — are eliminated. In the presence of inhibitors,  $\gamma\text{H2AX}/53\text{BP1}$  foci yield grows linearly, which indicates a pronounced modifying effect of DNA repair inhibitors on the formation of enzymatic DNA DSBs after exposure to  $^{60}\text{Co}$   $\gamma$ -rays (Fig. 6).

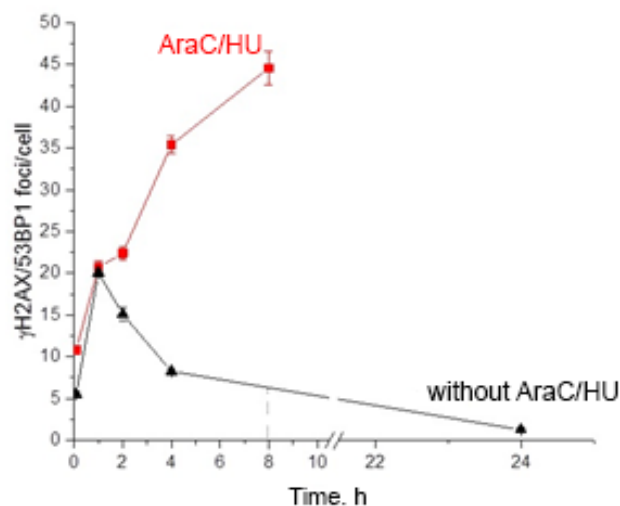


**Fig. 6.** Kinetics of  $\gamma\text{H2AX}/53\text{BP1}$  foci yield in human fibroblasts in the presence of AraC and HU after exposure to  $^{60}\text{Co}$   $\gamma$ -rays.

A qualitative analysis was performed of morphological changes in Purkinje neurons of the rat cerebellar cortex, which are easily identified without using specific morphological markers thanks to a unique anatomical organization of the cerebellar cortex [5]. It was established that the maximal yield of  $\gamma\text{H2AX}/53\text{BP1}$  foci in Purkinje neurons is formed 1 h after exposure (12  $\gamma\text{H2AX}/53\text{BP1}$  foci/nucleus); 4 h later, it decreases by 50%. 24 h after irradiation, only 2.5 foci/nucleus remains in nuclei, which points to effective DNA DSB repair. It was shown that the dose dependence of the frequency of  $\gamma\text{H2AX}/53\text{BP1}$  foci formation 1 h after exposure to  $^{60}\text{Co}$   $\gamma$ -rays is linear (Fig. 7).

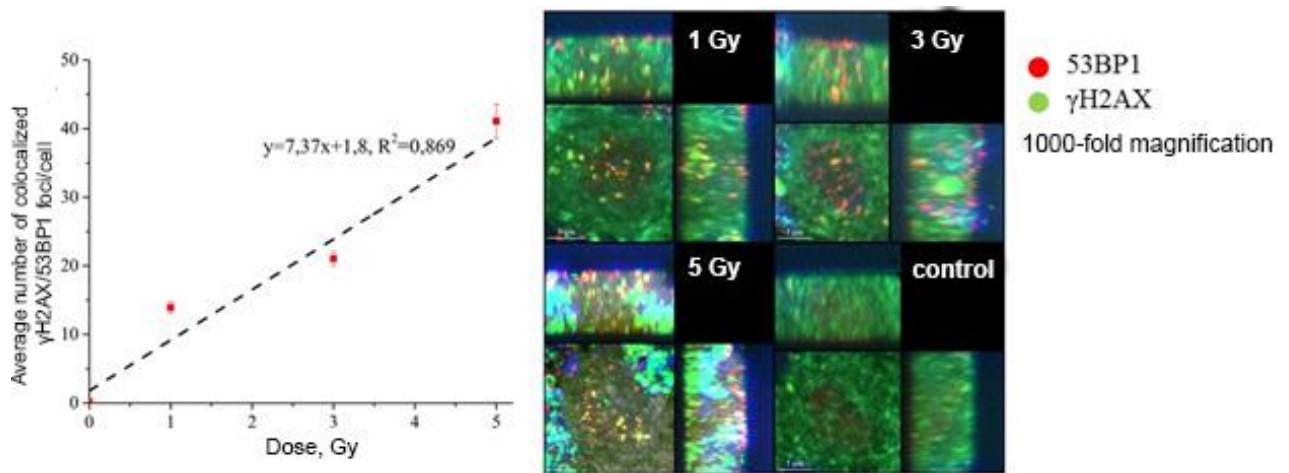


**Fig. 7.** A dose dependence of the number of radiation-induced  $\gamma$ H2AX/53BP1 foci in Purkinje cell nuclei 1 h after exposure.

The role was studied of radiation-induced reactive oxygen species (ROS) and reactive nitrogen species (RNS) in the induction of chromosomal aberrations in CAL51 cells of human breast carcinoma at high and low  $\gamma$ -radiation doses. It is generally thought that oxidative and nitrosative stress induced in cells by ionizing radiation causes DNA damage and cell death. Using antioxidants significantly moderates these adverse consequences. However, these compounds perform the key regulatory role at the physiological level. In particular, ROS and RNS activate quite a number of cytoprotective mechanisms aimed at cell homeostasis recovery and thus prevent oxidative and nitrosative stress development. It allows assuming that at high and low doses of ionizing radiation, the ROS and RNS effect on chromosome aberration yield can significantly differ. To check this suggestion, chromosome aberration yield after  $\gamma$ -exposure was studied in CAL51 cells in the presence of the antioxidant TEMPOL and nitrogen oxide interceptor PTIO. The aberrations were detected with the anaphase technique. An analysis of the data shown in Fig. 8 allowed concluding that at high doses oxygen and nitrogen radicals make a great contribution to chromosome aberration induction because radical neutralization in the presence of TEMPOL and PTIO leads to a decrease in aberrant cell yield, the modifiers' joint action having a synergetic effect. A different pattern is observed at a dose of 0.1 Gy. Nitrogen oxide neutralization has no influence on chromosome aberration yield; ROS yield suppression causes an insignificant increase in chromosome aberration yield, and the modifiers' joint action causes a sharp DNA damage increase. So, it was established that ROS and RNS perform a protective function at low doses, and using antioxidants can have negative consequences for the cell in this case.

Analysis of chromosomal aberrations in peripheral blood lymphocytes of *Macaca mulatta* monkeys was conducted after head irradiation with 170 MeV protons (3 Gy, LET  $\sim$  0.53 keV/ $\mu$ m) and, 48 days later, with accelerated 500 MeV/nucleon  $^{12}$ C ions (1 Gy, LET  $\sim$  10.6 keV/ $\mu$ m) [6]. It

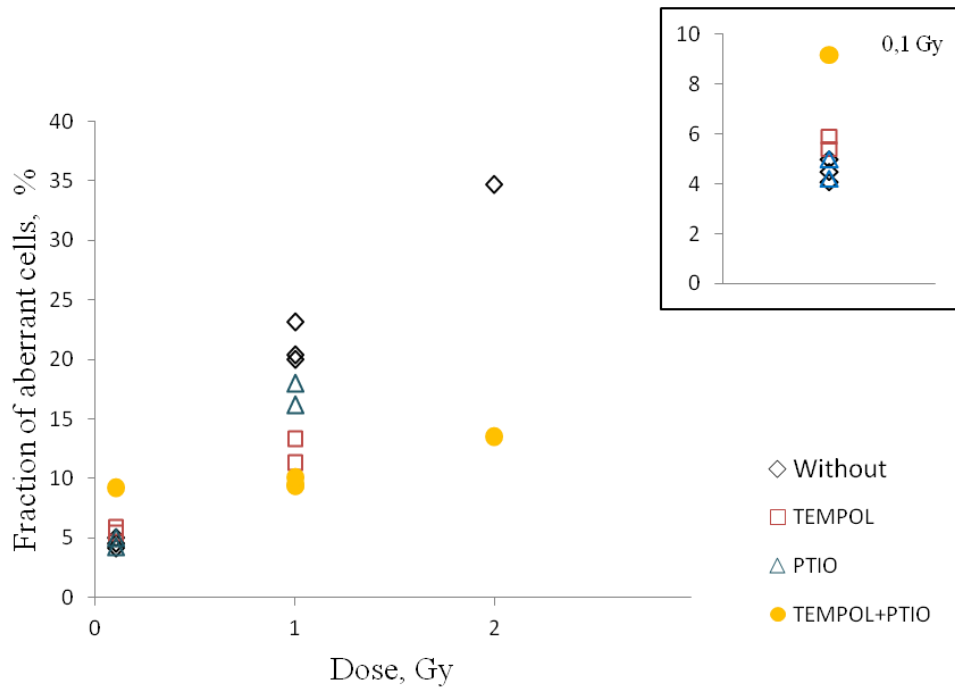


**Fig. 8.** The effect of ROA and RNS yield suppression (TEMPOL and PTIO, respectively) on the frequency of chromosomal aberrations induced by  $^{60}\text{Co}$   $\gamma$ -radiation.

was found that the number of chromosomal aberrations was monotonically decreasing during the whole study (454 days); this decline is well described by a logarithmic function (Fig. 9). After a chromosomal aberration elimination-based extrapolation of the obtained logarithmic curve to later

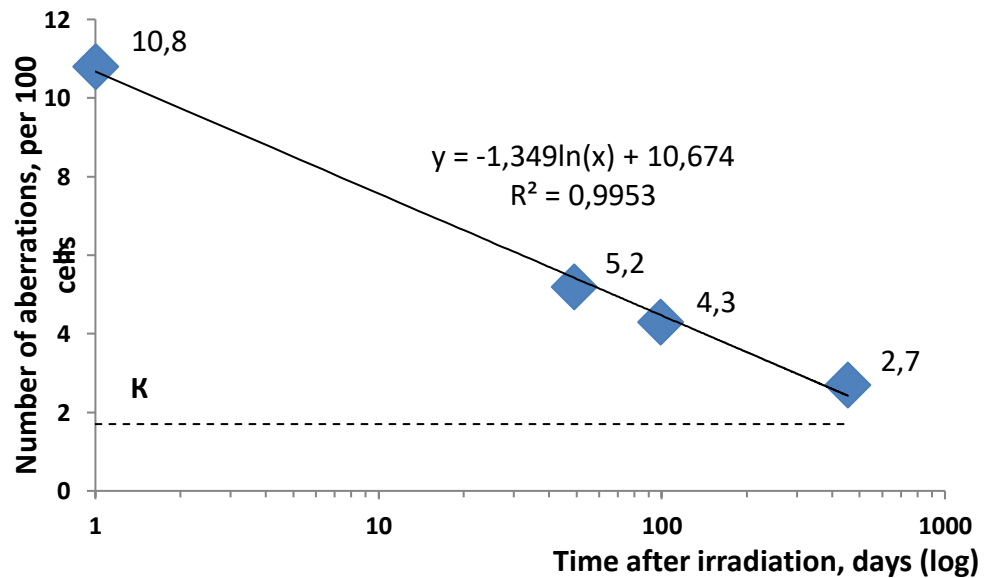


**Fig. 9.** The dynamics of the total number of chromosomal aberrations in blood lymphocytes of *Macaca mulatta* monkeys after head irradiation with 170 MeV protons (3 Gy) +  $^{12}\text{C}$  ions (1 Gy).

times, it can be assumed that the control sample's level of chromosomal aberrations would be reached approximately 2 years after exposure. Besides, a dose dependence was obtained of chromosomal aberration yield in monkeys' peripheral blood lymphocytes after *in vitro* exposure of blood samples to 170 MeV protons.

## 2.2. *Photoradiobiological research*

Research was continued on the role of Müller glial cells (MGC) in the mouse retina recovery mechanism. It was shown that retinal resistance that formed after a pre-exposure to 170 MeV protons at a dose of 1 Gy followed by a cytotoxic injection of methylnitrosourea correlates with a decrease in the photoreceptor apoptosis frequency (Fig. 10), DNA double-strand break yield, Caspase-3 expression, and MGC gliosis, which indicates a decrease in the level of cell damage and death in the retina.

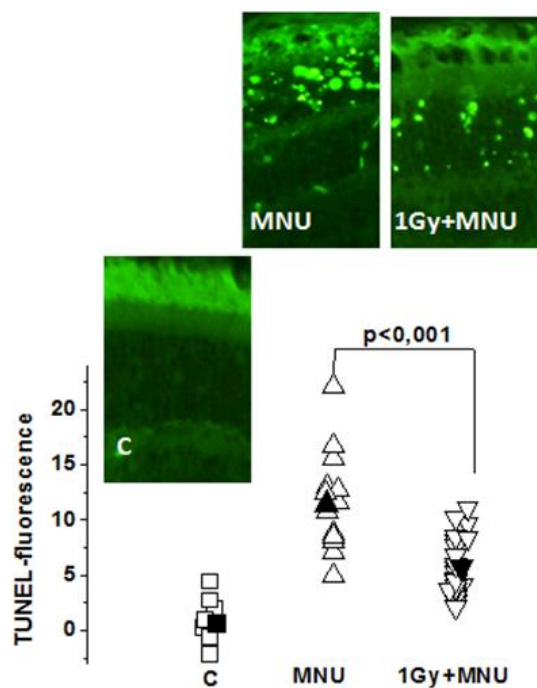


**Fig. 10.** The fluorescence intensity of the nuclear layer of the mouse retina photoreceptor cells in the control (C), 48 hours after a single 70 mg/kg methylnitrosourea injection (MNU), and after a combined action of 1 Gy of accelerated protons and a 70 mg/kg MNU injection.

A series of experiments were conducted jointly by the LRB JINR and Sofia University Kliment Ohridski. It was shown that when a mouse electroretinogram (ERG) is fully rectified after a visible light exposure, retinal functional activity recovers in 1—2 hours. It was also shown that a total mouse irradiation with 170 MeV protons and  $\gamma$ -rays at a dose of 5 Gy causes an irreversible decrease of the ERG amplitudes 8—9 months after the exposure (Fig. 11).

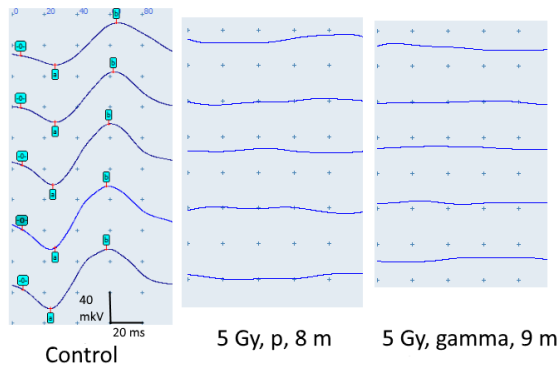


**Fig. 11.** Changes in a mouse ERG after a whole body irradiation with protons and  $\gamma$ -rays at a dose of 5 Gy.

### 2.3. *Radiation physiology and neurochemistry*

A cycle of research on the neurochemical indices of the rat brain after exposure to ionizing radiations of different quality was performed. With the highly efficient liquid chromatography technique, changes were evaluated in the levels of the key brain neuromediators (noradrenaline, dopamine, serotonin, and their metabolites) in rats of different age cohorts irradiated with 500 MeV/nucleon  $^{12}\text{C}$  ions at a dose of 1 Gy. It was shown that accelerated heavy charged particles induce changes in the functioning of the noradrenaline, dopamine, and serotonergic system 30 and 90 days after an exposure. The most pronounced differences between the irradiated and control animals were observed in the prefrontal cortex, nucleus accumbens, and hypothalamus, which points to an important role of these structures in the realization of the long-term effects of radiation exposure on the central nervous system functions. For a number of indicators of the content of monoamines and their metabolites in the brain, a decrease was observed in the intensity of the temporal changes in the prefrontal cortex, hypothalamus, and hippocampus of the irradiated rats. On the basis of these results, it was assumed that in the late post-irradiation period an active realization of the compensatory and recovery mechanisms takes place. At relatively low linear energy transfer (LET) of the particles — about 10 keV/ $\mu\text{m}$  — these mechanisms can lead to a partial recovery of the brain's functions damaged by radiation (Fig. 12). At higher LET, the compensatory and recovery mechanisms are less pronounced, and functional disorders increase with time [7].

Neurochemical research results were compared with animal behavior indices after irradiation. It was found that along with changes in monoamine metabolism, exposure to accelerated  $^{12}\text{C}$  ions leads to modifications of animals' motion and exploratory activity and changes in irradiated rats' anxiety indices (Fig. 13) [8].

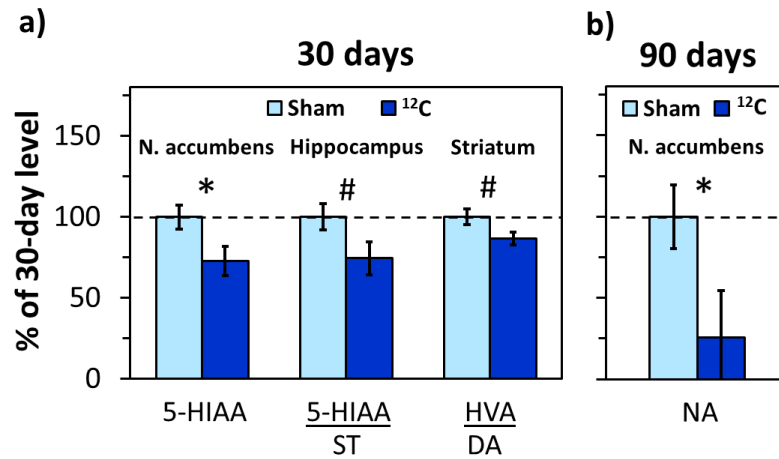


**Fig. 12.** Monoamine metabolism dynamics in rat brain structures after exposure to accelerated carbon ions ( $^{12}\text{C}$ , 500 MeV/nucleon, 1 Gy;  $\pm\text{SEM}$ ; \*  $p < 0.05$ ; #  $p < 0.1$ ; single-factor analysis of variance). The evaluation was obtained by comparing the respective data 30 (a) and 90 (b) days after irradiation. Monoamines and their metabolites are denoted as follows: DA — dopamine, ST — serotonin, NA — noradrenaline, 5-HIAA — 5-hydroxyindoleacetic acid, HVA — homovanilic acid, SI — sham irradiation (keeping the control rats in the same conditions as the irradiated ones but without radiation exposure).

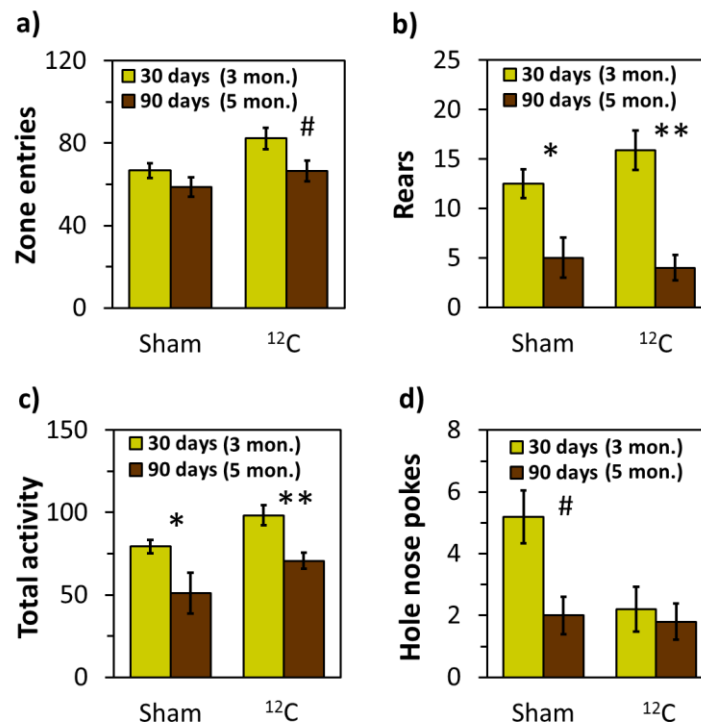


**Fig. 13.** The effect of accelerated carbon ions ( $^{12}\text{C}$ , 500 MeV/nucleon, 1 Gy) on the temporal dynamics of the open field test indices: (a) the number of the crossed zones, (b) the number of elevations, (c) total motion activity as a sum of zone crossings and elevations, and (d) the number of the acts of studying holes in the floor ( $\pm\text{SEM}$ ; \*  $p < 0.05$ ; \*\*  $p < 0.01$ ; #  $p < 0.1$  between 30 and 90-day indices; single-factor analysis of variance). In parentheses, the animals' age at the time of research is specified. SI — sham irradiation (keeping the control rats in the same conditions as the irradiated ones, but without radiation exposure).

A comparative study was conducted of the effect of 500 MeV/nucleon  $^{12}\text{C}$  ions and  $\gamma$ -rays at a dose of 1 Gy on the dynamics of age-related changes in monoamine exchange. It was shown that  $\gamma$ -radiation has a weaker effect on the age-related dynamics of neuromediator exchange than  $^{12}\text{C}$  ions. Based on this research, it was assumed that in the case of heavy ion exposure, more serious disorders in the functioning of the neuromediator systems lead to a higher intensity of the compensatory and recovery processes, which can cause a modification of the normal dynamics of the age-related changes during the studied post-irradiation period.

Modeling was done of a combined effect of the radiation and non-radiation space flight factors on rats' behavior and cognitive abilities as well as on monoamine and acetylcholine metabolism in the key structures of the rat brain [9-11]. With this purpose, a combined exposure to weightlessness, simulated by anti-orthostatic suspension, and radiation, represented by  $\gamma$ -rays and Bragg peak protons, was studied. An integrated evaluation of animals' behavior indices included the following tests: open field, Morris water maze, elevated plus maze, and passive avoidance. It was found that both with and without anti-orthostatic suspension, radiation caused rats' thigmotaxis attenuation (Fig. 14). A decrease in the learning ability related to working (but not spatial) memory damage was observed in response to anti-orthostatic suspension and a combined exposure. An analysis of monoamine metabolism showed that the serotonergic system is the most sensitive to the space flight factors modeled in the experiment. Compared with the animals that underwent only anti-orthostatic suspension, the irradiated rats and the rats that were subjected to

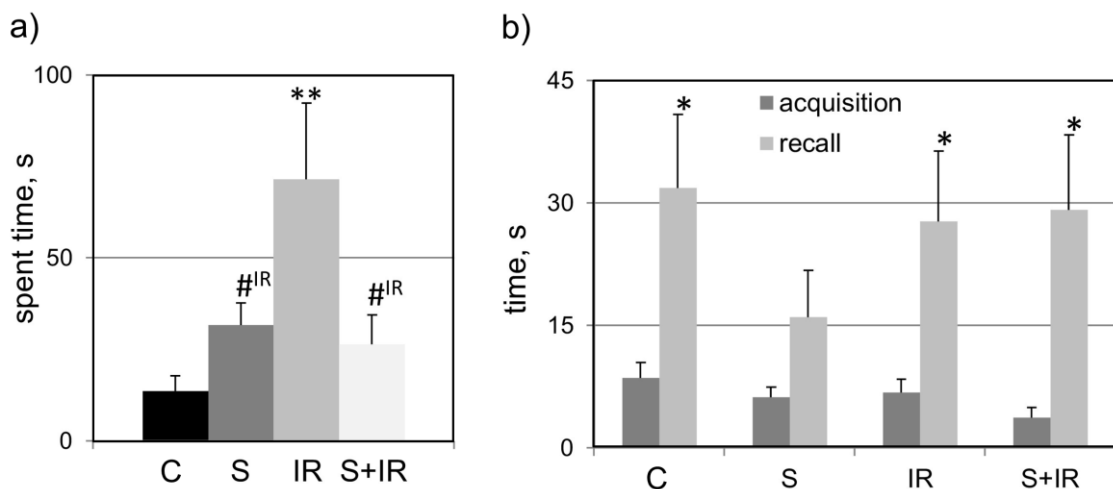


**Fig. 14.** (a) The combined effect of space flight factors on total spent time in the elevated plus maze test ( $\pm$ SEM; \*\*  $p < 0.01$ ; #  $p < 0.05$  by Duncan's test); (b) the passive avoidance test indices ( $\pm$ SEM; \*  $p < 0.05$  by a  $t$ -test). C — control animals; AOS — animals that were subjected to anti-orthostatic suspension modeling weightlessness; IR — animals exposed to ionizing radiation; AOS+IR — animals subjected to a combination of anti-orthostatic suspension and radiation exposure.

a combined exposure showed a much higher acetylcholine concentration in their hippocampus. In general, the results of this research point to an antagonistic effect of anti-orthostatic suspension and radiation exposure on the animals' cognitive functions and psycho-emotional condition.

#### **2.4. *Mathematical modeling of radiation-induced effects***

Modeling of heavy charged particle-induced genetic damage repair systems was continued. Results were published of the mathematical analysis of the mechanisms of the regulation of the functioning of the repair systems in bacterial cells and a comparative analysis of their efficiency [12], as well as modeling systems of repair of DNA double-strand breaks (DSBs) induced by  $\gamma$ -rays, neutrons, and charged particles in a wide linear energy transfer (LET) range [13].

Modeling was continued of the molecular mechanisms of heavy charged particle-induced disorders of central nervous system (CNS) structures and functions. Studying the early stages of nervous cell damage induced by high-energy heavy charged particles is of particular importance for explaining later CNS functional disorders. With the use of a Monte Carlo technique realized in the Geant4-DNA software tool, a computer simulation was done of physicochemical acts of charged particle interaction with separate cerebral neurons and a small neural network made up of 10 neurons (Fig. 15) [14-16]. Calculations were performed for  $^{12}\text{C}$  and  $^{56}\text{Fe}$  ions and protons of different energies in a relatively wide LET range — from several to hundreds of  $\text{keV}/\mu\text{m}$ . The topologies of the neurons and neural network in the CA1 region of the hippocampus were taken

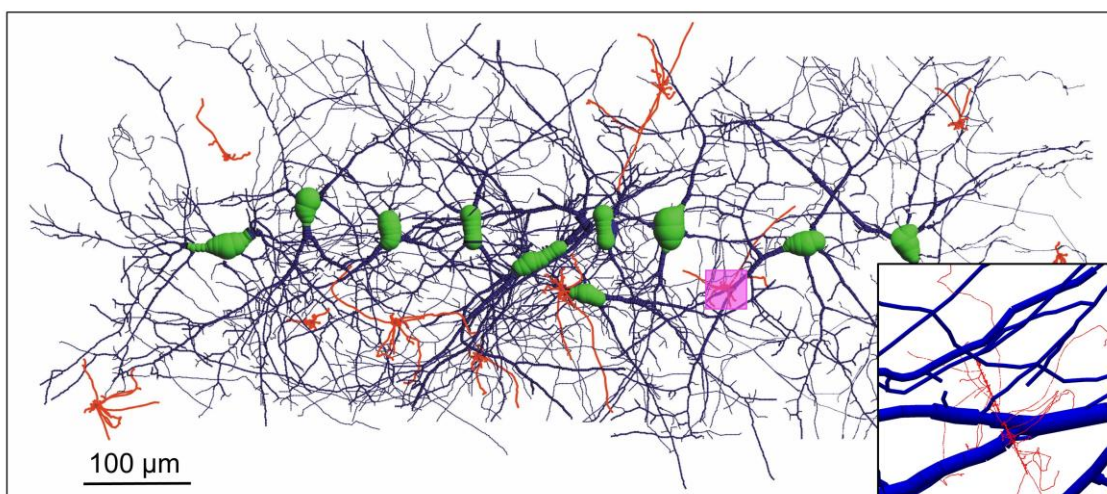


**Fig. 15.** A spatial model of a 10-cell neural network in the CA1 region of the hippocampus crossed by 10 tracks of 1000 MeV/nucleon  $^{56}\text{Fe}$  ions. The inset shows a zoom into the area marked purple. The  $^{56}\text{Fe}$  tracks are red.

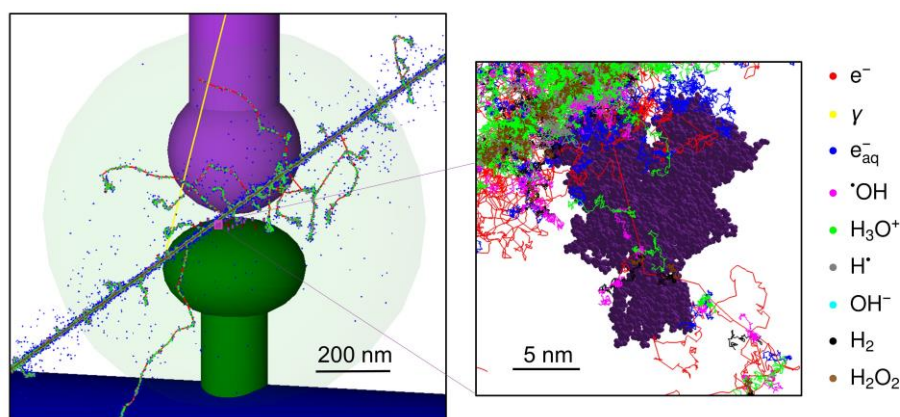


**Fig. 16.** Physicochemical processes in the structure of a 100 MeV/nucleon  $^{56}\text{Fe}$  ion track crossing a synaptic contact zone. Shown are a presynaptic axon (purple) and a postsynaptic dendrite spine (green) with the NMDA and AMPA receptors (purple and maroon, respectively). The inset on the right shows a zoom into a fragment of a model of the NMDA receptor with segments of secondary particle tracks and water radiolysis products. The dots of different colors denote the spatial localization of the radiolysis products.

from the known data available at the NeuroMorpho.org database. The spatial distributions of the local dose and energy transferred by charged particles to the sensitive structures of the neuron were calculated; radiolysis product yield was estimated. Special attention was paid to the processes of energy deposition in synaptic contacts (Fig. 16). The average number was calculated of energy deposition events in small volumes ( $359.9$  and  $429.8 \text{ nm}^3$ ) corresponding to the NMDA and AMPA receptors (Fig. 17a). An estimation of radiolysis product yield in neurons (Fig. 17b) allows assuming that the observed increase in the reactive oxygen species level can be one of the causes of the oxidative damage to synaptic structures, which violates the normal transmission of a nerve impulse between cells. The results of this study suggest that neuron morphology is an important factor determining the accumulation of the local exposure dose and radiolysis products in cells. To calculate the dysfunctions of the synaptic receptors, it is necessary to know both the spatial distribution of damage emerging after charged particle passing and the temporal dynamics of the closure and opening of the ion channel of the formed structure during functional activity. To this end, molecular dynamics methods were used [17]. A model of the NMDA glutamate receptor was taken from the PDB base (structure 4TLM). Some parts of the system were reconstructed by the MODELLER program and refined by the VMD software package. The ion channel radius changes were calculated with the HOLE program. The obtained results make it possible to calculate theoretically the radiation damage to the receptors and the corresponding synaptic transmission change, which is necessary for the analysis of the disorders of neural networks' neurophysiological activity.

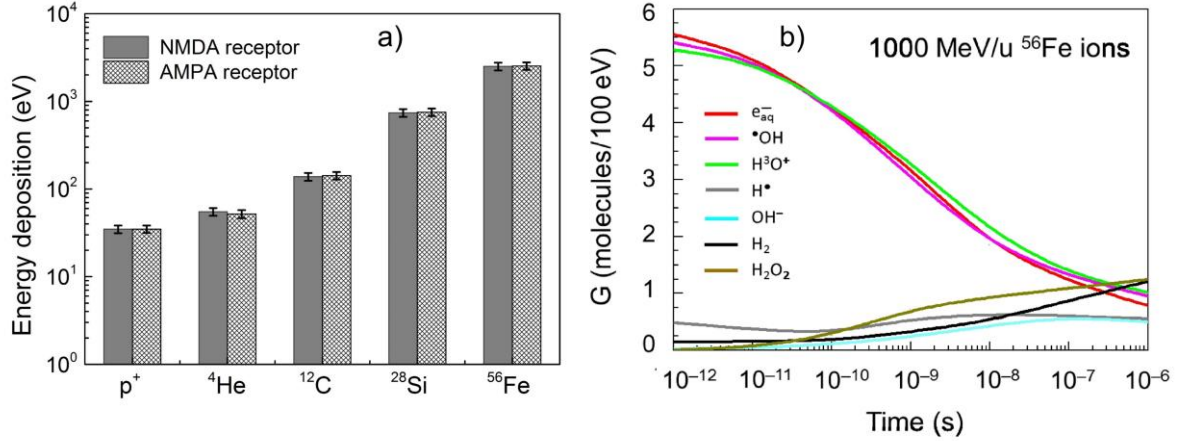


**Fig. 17.** (a) Average energy deposition in NMDA and AMPA synaptic receptor structures for the following 1000 particles with an energy of 1000 MeV/nucleon:  $p^+$ ,  $^4\text{He}$ ,  $^{12}\text{C}$ ,  $^{28}\text{Si}$ , and  $^{56}\text{Fe}$ . (b) Water radiolysis product yield ( $G$ ) per 100 eV for a 1000 MeV/nucleon  $^{56}\text{Fe}$  ion crossing it. The chosen time interval corresponds to the chemical stage of particle track evolution.

A model of intracellular signal transport along the microtubes of the nervous cell axons was proposed (Fig. 18) [18-20]. The framework's dynamics description is based on a quasi-one-dimensional nonlinear chain model; for the oscillations of the microtube surface-located ends consisting of carboxylic groups (C-termini), an analogy with smectic liquid crystals is used.

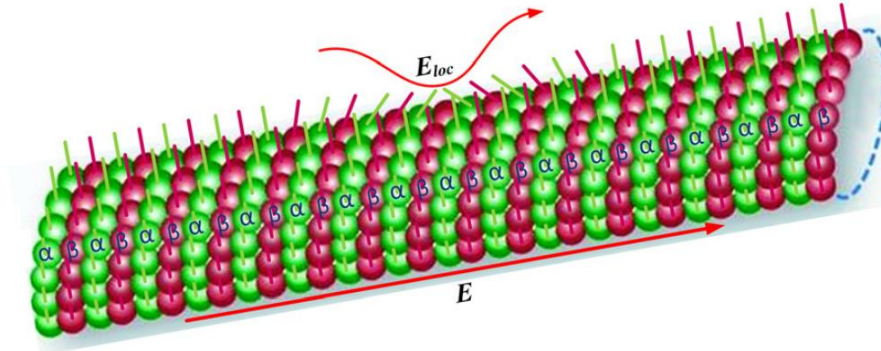


**Fig. 18.** A schematic of a ferroelectric model of a microtube as a liquid crystal layer rolled into a cylinder. The G-termini are shown as rods. The microtube forms a giant dipole with the internal electric field  $E$ . The localized signal wave is denoted as the corresponding associated field  $E_{\text{loc}}$ .

For the considered degrees of freedom, nonlinear solutions of the kink and breather types were obtained and analyzed; the characteristic parameters and propagation velocity were determined. The stability of the found solutions was calculated. The influence was analyzed of the microtube-associated proteins — in particular,  $\tau$ -protein — and modification of C-termini on signal propagation. The obtained results clear up the possible mechanisms of cytoskeleton degradation and disorders of intracellular signaling induced by a radiation or chemical exposure.

The development of mathematical models of neural networks and structures is an extremely important task in the analysis of the radiobiological effects of accelerated charged particles. The dynamics was studied of the time-space structure of prefrontal cortex neurons during working memory functioning [21]. The proposed biophysical model is a neural network of 36 interneurons and 144 pyramidal neurons, which are interconnected by excitatory and inhibitory synapses. Each neuron's morphology is taken into account, consisting of the soma and dendrite structure with the corresponding distribution of ion channels. When information on some object is received, spatially ordered structures with high cell activity emerge in the modeled brain's region (Fig. 19). The model

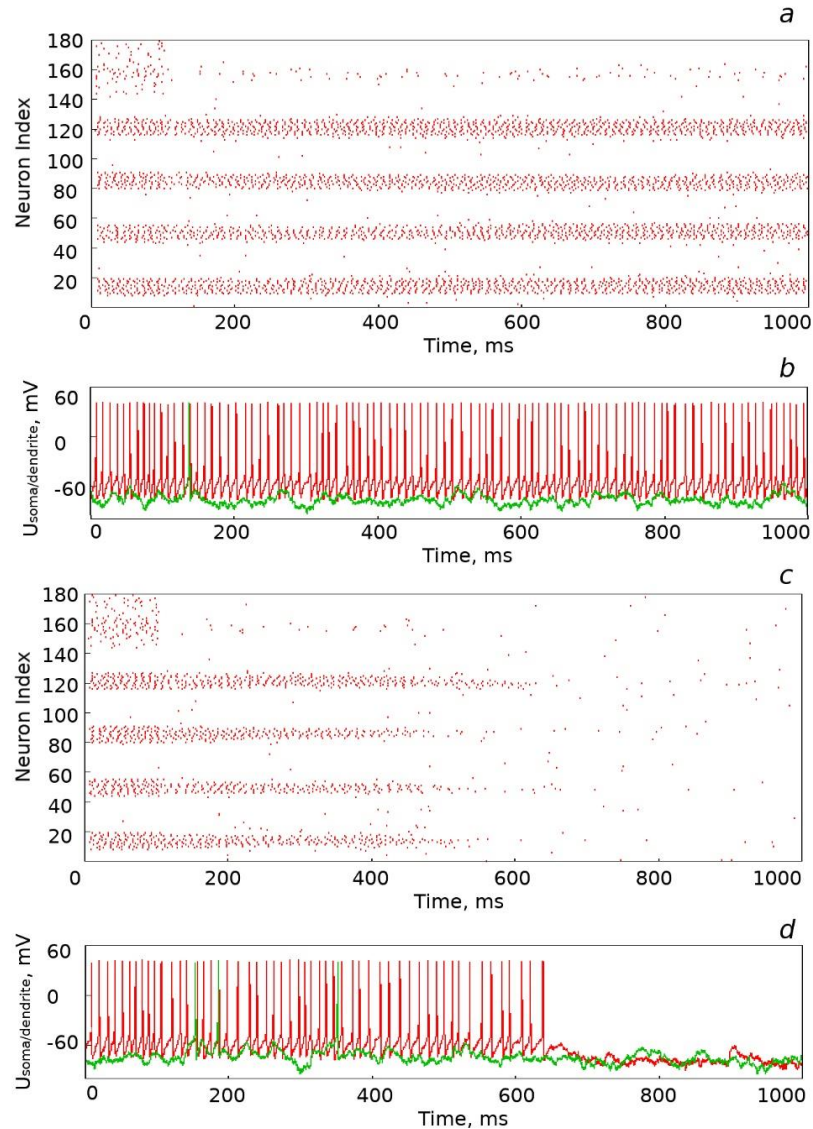


**Fig. 19.** A calculation of pattern generation from operation potential pulses during the functioning of working memory: (a) a rastergram showing the coordinate and time of pulse generation (dots); (b) the temporal dynamics of the operation potential  $U$  on the soma (the red curve) and dendrites (the green curve) of an isolated neuron. (c, d) Changes in neural network parameters after exposure to 600 MeV/nucleon  $^{56}\text{Fe}$  ions at 0.3 Gy.

includes the radiation-induced changes in the synaptic receptor number and ion channel conductivities evaluated on the basis of experimental data. In the course of calculations, an absorbed dose threshold was found, above which the stability of the time-space structures specific for the given network is lost.

A model was developed of the neuron population of the CA3 region of the hippocampus taking into account the membrane properties and spatial geometry of the synaptic contacts [22]. A special feature of the model is a detailed record of each single neuron's spatial structure, which holds up to 19 segments. Prospects are thus opened for the further development of the model's radiobiological aspects with the use of microdosimetry methods with a view to the evaluation of energy deposition in tracks of charged particles of different energies. Both in isolated neurons and in their population, the operation potential is generated in a burst mode, the frequency of which increases with external stimulus enhancement. Later, this model is going to be the basis of a more detailed analysis of the electrophysiological activity of the hippocampus neurons and radiation-induced damage to spatial memory.

## ***2.5. Radiation protection physics and radiation research***

Two radiobiological research sessions were conducted at the MC400 cyclotron, the Laboratory of Nuclear Reactions: with 36 MeV/nucleon  $^{11}\text{B}$  nuclei (23—24 January 2016) and with 50 MeV/nucleon  $^{20}\text{Ne}$  nuclei (30 March 2016). A  $\Delta E$ -E spectrometer for monitoring the charge composition of an ion beam was tested at the LRB's facility Genome-M.

Work was continued on the prediction of the radiation conditions during NICA complex operation. A number of specific tasks were performed, including the evaluation of the stripping target activation, dose rates near the booster — Nuclotron transport channel, exposure of the electronics mounted near the arches of the external wall of the collider canyon, exposure and activation of the system's high-frequency (HF) resonators, the possibility of using an iron — cobalt alloy for making the HF cores, etc. The next important stages of solving the radiation safety issues at the NICA complex are the calculation of the upper shielding of the Nuclotron tunnel and estimation of the contribution of the BM@N experiment (Building 205) to the radiation conditions at the adjacent territory.

In a joint effort with specialists of the Medical Technical Complex (MTC), the Laboratory of Nuclear Problems, a reference field of secondary neutrons from the MTC carbon absorber was generated for long-term fractionated (quasi-chronic) irradiation of laboratory animals, and first exposures of mice were performed. The component and spectral composition of the field was

calculated with the Monte Carlo software package MCNPX for simulating radiation transport in matter.

In 2016, in cooperation with specialists from the Space Research Institute of the Russian Academy of Sciences, a great amount of equipment testing for future missions Luna-Glob, Luna-Resource, BepiColombo, and ExoMars was performed at the planetary soil model of the DAN (Dynamic Albedo of Neutrons) experimental stand.

## 2.6. *Studying cosmic matter on Earth and in nearby space*

Research was continued on the synthesis of prebiotic compounds from formamide with meteorites as catalysts under exposure to radiation. Materials were published on irradiation with boron ions [23]. 170 MeV proton irradiation of mixtures of formamide and different meteorite samples was repeated. Another type of sample analysis was performed: Raman spectroscopy. 18 samples of meteorite matter and terrestrial minerals were used in the experiment (the meteorites: Campo del Sielo, Canyon Diablo, Sikhote-Alin, Seymchan, NWA4482, NWA2828, Gold Basin, Dhofar959, NWA1465, NWA5357, Al Haggounia, and Chelyabinsk; the minerals: covellite CuS, chalcopyrite CuFeS<sub>2</sub>, montmorillonite KSF, and Al-pillared montmorillonite KP-30) in a mixture with formamide. This research was done in collaboration with the Biophotonics Laboratory of the Institute of Electronics, the Bulgarian Academy of Sciences. The study was based on using a state-of-the-art inVia Qontor Raman microscope (the Renishaw company) at the Faculty of Nano- and Biomedical Technologies, Saratov Chernyshevsky State University, with which the LRB's Bulgarian colleagues are cooperating. The acquired spectra are being analyzed. Preliminary results indicate that nucleic bases and nucleosides were present the reaction mixtures (Table 1).

Experiments were conducted on the synthesis of DNA and RNA component nucleosides by irradiating "nucleic base + sugar" mixtures with a 170 MeV proton beam. As sugars, ribose and 2-

**Table 1.** Results of the irradiation of "formamide + meteorite/mineral" mixtures obtained by Raman spectroscopy: the observed nucleic bases and nucleosides.

Absent/ **present**

Uracil	Cytosine	Hypoxanthine	Adenine	Guanine	Purine	4,6-DHP	Mannose	2,6-Diaminopurine	
Orotic acid	Isocytosine	4(3H)pyrimidone	Thymine	AHMN	DAMN	4-AMI	Thymidine	2'-Deoxyribose	Ribose
Glucose	Galactose	3(OH)pyridine	Inositol	Arabitol	Uridine	Cytidine	Adenosine	2'-Deoxyglucose	

deoxyribose were used. A "nucleoside + phosphate group" mixture was exposed to the same radiation in search of a possible synthesis of nucleotides that are DNA and RNA building blocks. The results were analyzed in Viterbo, Italy. Based on the preliminary results, it can be confidently said that irradiation of an "adenine + deoxyribose" mixture (Fig. 20) yielded, besides other molecules, deoxyadenosine and polyribosylated adenosine (Fig. 21).

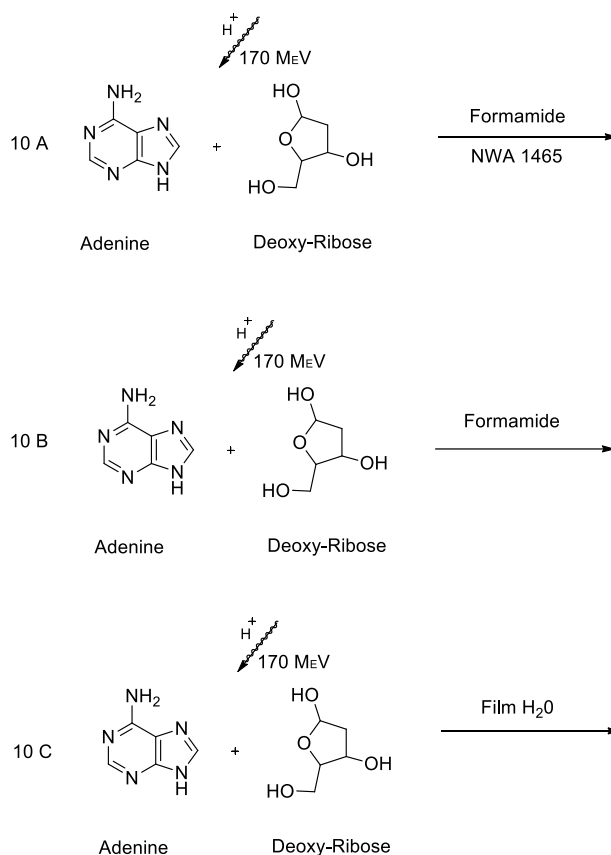


**Fig. 20.** A scheme of the irradiation of an adenine — deoxyribose mixture.

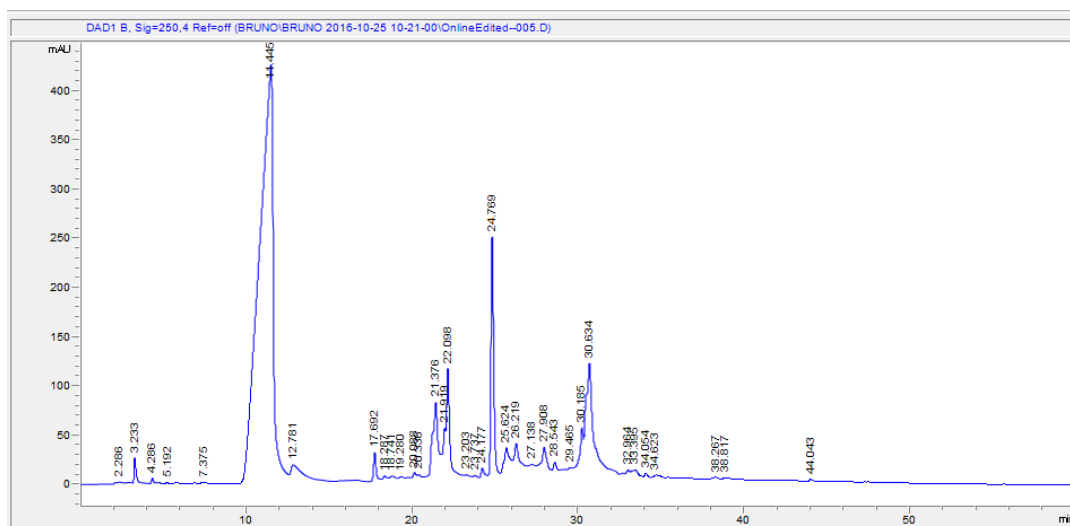


**Fig. 21.** A high-pressure liquid chromatography spectrum of an irradiated mixture "adenine + deoxyribose + formamide + NWA1465."

A micropaleontological study of early Precambrian rocks was done at Borisyak Paleontological Institute of the Russian Academy of Sciences. All bacterial paleontology analyses were made using the following scanning electron microscopes: CamScan-4 with a Link-60 microanalyzer; Zeiss EVO 50 with an Inca Oxford (350) X-ray microanalyzer; and TESCAN VEGA II ZMU with an X-ray energy dispersive microanalysis system INCA ENERGY 450. Only fresh cleavages of rocks (both ancient and modern) were studied — sometimes, slightly acid-etched. It should be noted that pseudomorphs, not microorganisms themselves, were the subject of research in all cases.

Research on the most ancient residual as well as Archean and early Proterozoic ferruginous quartzites of Karelia, the Kola Peninsula, and the Kursk Magnetic Anomaly was continued soils (Fig. 22) [24-27]. New data were obtained on the biogenic origin of minerals. The role of life was evaluated in relation to the concentration of minerals on Earth. Issues of the settlement of lava flows [28] and land colonization by microorganisms [29, 30] were examined.

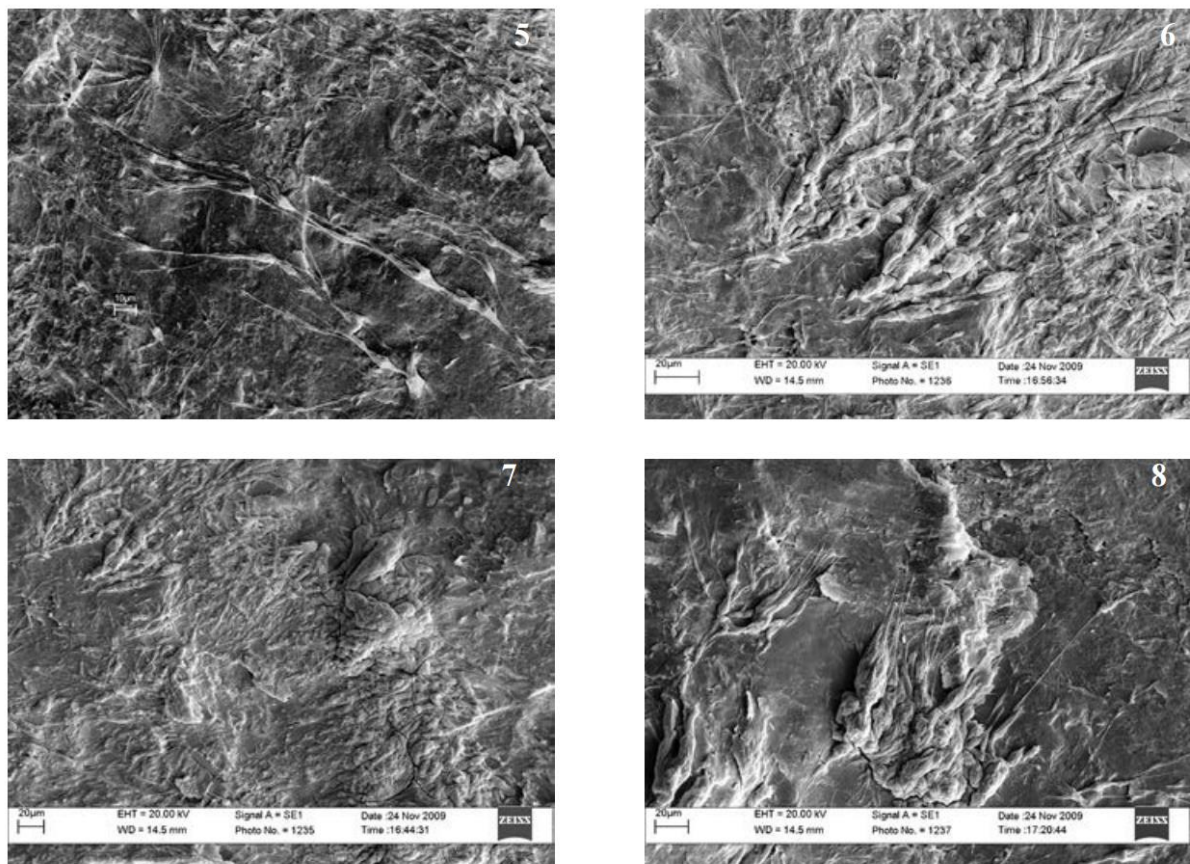


**Fig. 22.** Highly organized fossilized algaes *Gazavazhinia antiqua* Rozanov et Astafieva, 2013 (Imandra-Varzuga, PR<sub>1</sub>, 2.45 billion years): 5—7 — amply ramified main stems (about 10 μm in diameter) and ramified side branches (about 5 μm in diameter) are seen; 8 — flattened rounded bases, or patches (more than 50 μm in size), by means of which algae stuck to the substrate.

In early Proterozoic ferruginous quartzites of the Kursk Magnetic Anomaly (the Lebedinsky mine; limonite-martite ores and striated ferruginous quartzites of the Korobkovsky ore deposit), fossilized cyanobacteria were found, represented by trichomes merged into a single cover [24]. The minerals are deposited *in situ*. Morphologically, they are close to the modern representatives of the genus *Microcoleus*.

In striated ferruginous quartzites aged 2.7-2.8 billion years (the Archean Eon) from deposits in Karelia and the Kola Peninsula, microfossils of an apparently bacterial origin were found [27]. On the basis of an evaluation of organic carbon content and balance calculations, it was established that the formation of the studied Archean ferruginous quartzites took place in a medium enriched with organic matter. A comparative analysis of the morphology of modern and Neoproterozoic microorganisms suggests a bacterial origin of some amount of magnetite in the studied quartzites.

The results of microfossil research indicate that the biogenic factor played an important role in the formation of sedimentary early Proterozoic ferruginous quartzites of the Kursk Magnetic Anomaly. It was confirmed by the finds of cyanobacteria and abundant glycoalyx in fossil samples. It follows from here that sedimentary ferruginous quartzites were being deposited in the photic zone conditions — that is, in shallow water — and O<sub>2</sub> content in the atmosphere was quite high.

In early Precambrian Keiv proto-schists (the Kola Peninsula), nanobacteria deposited *in situ* were found. It is suggested that the presence of nanobacteria points to the involvement of the biological factor in the formation of host rocks; also, the presence of biofilms and nanobacteria suggests that the conditions of the external medium were unfavorable for bacterial life.

### ***3. Conferences and education***

In 2016, the Laboratory's researchers participated in 14 scientific conferences in Russia and 10 conferences in different countries of the world. Jointly with the Scientific Council on Radiobiology of the Russian Academy of Sciences, a three-day conference was held entitled "Urgent Problems of Radiobiology and Astrobiology. Genetic and Epigenetic Effects of Ionizing Radiations." Its participants were about 100 scientists of institutes and research organizations of Russia, Italy, and the U.S. Discussed were urgent issues of space radiobiology, astrobiology, radiation genetics, molecular and cell radiobiology, and data on the mechanisms of the formation of genetic and epigenetic changes in the genome.

The education process continued at the Department of Biophysics of Dubna University. The Department's current total enrolment includes 34 students and 7 postgraduates. Bachelor's education is given in the field of Nuclear Physics and Technology represented by the program Human and Environmental Radiation Safety; Master's education is given in the field of Physics

represented by the program Radiation Biophysics and Astrobiology, and postgraduate education is given in the specialty of Radiobiology. In 2016, eight students were enrolled in the Bachelor's program; five students continued their Master's program. Six students successfully completed education and received their Master's diplomas in the field of Physics (the program Radiation Biophysics and Astrobiology).

In 2016, Yulia Vinogradova, a Junior Scientist at the LRB, defended her Candidate's thesis "Research on Mouse Retina Damage and Recovery after Exposure to Accelerated Protons and Methylnitrosourea" and was awarded Moscow Oblast Governor's Prize in Science and Innovation for Young Scientists and Specialists for her work "Research on the Structural and Functional Recovery of the Mouse Retina after Retinotoxic Exposure to Ionizing Radiation and Alkylating Agents."

## Reference

1. *Zadneprianetc M., Boreyko A. V., Bulanova T., Falk M., Falková I., Davidkova M., Ježková L., Kozubek S., Krasavin E. A., Kruglyakova E., Smirnova E., Valentová O.* Spatiotemporal analysis of  $\gamma$ H2AX/53BP1 foci after high- and low-LET irradiation. // The 42nd Annual Meeting of the European Radiation Research Society ERRS 2016. 4—8 September 2016. Amsterdam, Netherlands. Book of abstracts. P. 107.
2. *Kruglyakova E.A., Boreyko A.V., Bulanova T.S., Zadnepryanets M.G., Ježková L., Smirnova E.V.* The effect of radiation quality on the formation of DNA damage and cell reactions in human fibroblasts. // 5<sup>th</sup> Annual Conference of Young Scientists and Specialists. Alushta, Russia, 2016 (in Russian) <http://indico.jinr.ru/contributionDisplay.py?contribId=54&sessionId=10&confId=89>
3. *M.G. Zadnepryanets, A.V. Boreyko, T.S. Bulanova, L. Ježková, E.A. Krasavin, E.A. Kruglyakova, E.V. Smirnova.* Space and time analysis of  $\gamma$ H2AX/53BP1 foci in accelerated ion tracks. // 7<sup>th</sup> International School on Molecular Genetics for Young Scientists "Genomics and Biology of Living Systems," 14—18 November 2016, Zvenigorod. Book of Theses, p. 31 (in Russian).
4. *Dubničková M., Kuzmina E.A., Chausov V.N., Ravnachka I., Boreyko A.V., Krasavin E.A.* The effects of Lipid A on gamma-irradiated human peripheral blood lymphocytes in vitro // *Phys. Part. Nuclei Lett.* (2016) 13: 274
5. *Bulanova T. S., Jezkova L., Kruglyakova E. A., Zadneprianetc M. G., Smirnova E. V., Boreyko A. V.* Formation and repair of DNA double-strand breaks in brain cells of Sprague Dawley rats after  $^{60}\text{Co}$   $\gamma$ -rays irradiation. // *PEPAN Letters*, special issue 2017. Submitted.
6. *Blaha, P.; Koshlan, I.V.; Koshlan, N.A.; Govorun, R.D; Elsha, D.V.; Bogdanova, J.V.; Krasavin, E.A.* HPRT mutant induction and analysis in V79 cells after exposure to ionizing radiation with different qualities. // In the Abstract Book of the 62<sup>nd</sup> Radiation Research Society Meeting. Kona, Hawaii, USA, 16-19 October 2016. p. 258.
7. *O. Belov, K. Belokopytova, A. Bazyan, V. Kudrin, V. Narkevich, A. Ivanov, Yu. Severiukhin, G. Timoshenko, E. Krasavin.* Exposure to  $^{12}\text{C}$  particles alters the normal dynamics of brain monoamine metabolism and behaviour in rats // *Physica Medica, European Journal of Medical Physics.* 2016, Vol. 32. No 9, pp. 1088—1094.
8. *K.V. Belokopytova, O.V. Belov, V.S. Kudrin, V.B. Narkevich, E.A. Krasavin, G.N. Timoshenko, A.S. Bazyan.* Monoamine exchange dynamics in the rat brain structures at late

- times after accelerated carbon ion exposure // *Neurochemical Journal*. 2016, Vol. 33, No. 2, pp. 147—155 (in Russian).
9. *Kokhan V.S., Matveeva M.I., Bazyan A.S., Kudrin V.S., Mukhametov A., Shtemberg A.S.* Combined effects of antiorthostatic suspension and ionizing radiation on the behaviour and neurotransmitters changes in different brain structures of rats // *Behavioural Brain Research*. Available online 21 October 2016. <http://dx.doi.org/10.1016/j.bbr.2016.10.032> pp.. 1–11
  10. *Kokhan V.S., Matveeva M.I., Mukhametov A., Shtemberg A.S.* Risk of defeats in the central nervous system during deep space missions // *Neurosci Biobehav Rev*. 2016, Vol. 71, pp. 621—632.
  11. *Bazyan A.S.* Motivational and emotional conditions: structural, system, neurochemical, molecular, and cellular mechanisms. // *Physiology-Usppekhi*. 2016, Vol. 47, No. 1, pp. 15—33 (in Russian).
  12. *Bugay A.N., Vasilyeva M.A., Parkhomenko A.Yu., Krasavin E.A.* Mathematical Analysis of Regulatory Networks and Damage Repair Efficiency in Bacterial Cells // *Genetics, Evolution and Radiation (Crossing Borders, The Interdisciplinary Legacy of Nikolay W. Timofeeff-Ressovsky)*, Eds.: Korogodina V.L., Mothersill C.E., Inge-Vechtomov S.G., Seymour C.B. Springer International Publishing AG. 2016, pp.175—186.
  13. *Fourie H., Slabbert J.P., Belov O.V., Newman R., Panina M.S., Rossouw N.* Estimating the effectiveness of high LET radiations to induce damage to DNA in human lymphocytes and modelling the repair thereof // *Physica Medica*. 2016, Vol. 32, p.155. <http://dx.doi.org/10.1016/j.ejmp.2016.07.051>
  14. *Bayarchimeg L., Belov O.V., Batmunkh M., Lkhagva O.* Modeling of synaptic receptors under irradiation with charged particles // *Mongolian Journal of Physics*. 2016. <http://mnglps.mn/index.php/en/> (in press)
  15. *Belov O.V., Batmunkh M., Incerti S., Lkhagva O.* Radiation damage to neuronal cells: Simulating the energy deposition and water radiolysis in a small neural network // *Physica Medica*. 2016, Vol.32, pp.1510—1520.
  16. *Batmunkh M., Belov O.V., Bayarchimeg L., Lkhagva O.* Radiation effects in the central nervous system: Simulation technique and practical applications // *Mongolian Journal of Physics*. 2016. <http://mnglps.mn/index.php/en/> (in press)
  17. *Dushanov E.* Ion channel dynamics of glutamate ionotropic receptors in synaptic transmission processes. // 23<sup>rd</sup> International Conference "Mathematics. Computer. Education." Dubna, 25—30 January 2016. Book of Theses. Vol. 23, p. 69 (in Russian)
  18. *Sekulic D.L., Sataric B.M., Zdravkovic S., Bugay A.N., Sataric M.V.* Nonlinear dynamics of C-terminal tails in cellular microtubules // *Chaos*. 2016, Vol.26, p. 073119.
  19. *Zdravkovic S., Zekovic S., Bugay A.N., Sataric M.V.* Localized modulated waves and longitudinal model of microtubules // *Applied Mathematics and Computation*. 2016, Vol. 285, pp.248—259.
  20. *Zdravkovic S., Bugay A.N.* Why are Biological Systems Nonlinear? // *Nonlinear Phenomena in Complex Systems*. 2016, Vol.19, No.1, pp.71—79.
  21. *Bugay A.N.* Radiation induced dysfunction in the working memory performance studied by neural network modeling // *Belgrade BioInformatics Conference 2016*. 20—24 June 2016. Book of Abstracts, p. 50.
  22. *Batova A.S., Bugay A.N., Parkhomenko A. Yu.* Approaches to the mathematical modeling of hippocampus neurons' electrophysiological activity. // *JINR News*, 2016, No. 3, pp. 26—29 (in Russian).
  23. *R. Saladino, E. Carota, G. Botta, M. I. Kapralov, G. N. Timoshenko, A. Yu. Rozanov, E.A. Krasavin, E. Di Mauro* «First Evidence on the Role of Heavy Ion Irradiation of Meteorites and Formamide in the Origin of Biomolecules», *Origins of Life and Evolution of Biospheres*, pp 1–7, 2016.

24. *Rozanov A.Yu., Astafyeva M.M., Zaytseva L.V., Alfimova N.A., Felitsyn S.B.* Cyanobacteria (?) in ferruginous quartzites of the Kursk Magnetic Anomaly. // *Dokl. Akad. Nauk.* 2016, Vol. 470, No. 3, pp. 1—3 (in Russian).
25. *Astafyeva M.M.* The most ancient weathering rinds and the problem of the bacterial colonization of land. // *Paleontology. Stratigraphy. Astrobiology. Marking the 80<sup>th</sup> birthday of A.Yu. Rozanov.* Borisyak Paleontological Institute of the Russian Academy of Sciences, Moscow, 2016, pp. 31—43 (in Russian).
26. *Astafyeva M.M.* New results of bacterial paleontology research. // The 100<sup>th</sup> anniversary of the Russian Paleontological Society. Problems and prospects of paleontological research. Proceedings of the 62<sup>nd</sup> session of the Paleontological Society. St. Petersburg, 2016, pp. 17—18 (in Russian).
27. *Astafyeva M.M.* First results of a bacterial paleontology study of early Precambrian ferruginous quartzites of Karelia and the Kola Peninsula. // Proceedings of the Round-Table Meeting "Topical Issues of Radiobiology and Astrobiology. Genetic and Epigenetic Effects of Ionizing Radiation." Dubna, Russia, 9—11 November 2016, pp. 91—93 (in Russian).
28. *Astafyeva M.M.* The early Earth: lava flows and the possibility of life. // Colloquium "Earth at the Early Stages of Solar Planetary System Development." Sternberg Astronomical Institute at Moscow State University, 28—30 November 2016 (in Russian).
29. *Astafyeva M.M.* Colonization of land. // The 2<sup>nd</sup> All-Russia Conference on Astrobiology (Life in the Universe: Physical, Chemical, and Biological Aspects). Pushchino, Russia, 5—9 June 2016, pp. 39—40 (in Russian).
30. *Astafyeva M.M.* Early colonization of land by microorganisms. // Proceedings of the 2<sup>nd</sup> All-Russia Paleophycological Conference "Algae in Biosphere Evolution." 2016, pp. 19—22 (in Russian).